Effect of the stress field of an edge dislocation on carbon diffusion in α-iron: Coupling molecular statics and atomistic kinetic Monte Carlo

R. G. A. Veiga and M. Perez
INSA Lyon, Laboratoire MATEIS, Université de Lyon, UMR CNRS 5510, 25 Avenue Jean Capelle, F69621 Villeurbanne, France

C. S. Becquart
Unité Matériaux et Transformations (UMET), Ecole Nationale Supérieure de Chimie de Lille, UMR CNRS 8207, Bat. C6, F59655 Villeneuve d'Ascq Cedex, France
and Laboratoire commun EDF-CNRS Etude et Modélisation des Microstructures pour le Vieillissement des Matériaux (EM2VM)

C. Domain
Recherche et Développement, Matériaux et Mécanique des Composants, EDF, Les Renardières, F77250 Moret sur Loing, France
and Laboratoire commun EDF-CNRS Etude et Modélisation des Microstructures pour le Vieillissement des Matériaux (EM2VM)

S. Garruchet
Laboratoire de Physico-Chimie des Surfaces, UMR CNRS-ENSCP 7045, Ecole Nationale Supérieure de Chimie de Paris, 11 Rue Pierre et Marie Curie, 75005 Paris, France

(Received 12 April 2010; revised manuscript received 22 June 2010; published 9 August 2010)

Carbon diffusion near the core of a $[111](\bar{1}01)$ edge dislocation in α-iron has been investigated by means of an atomistic model that brings together molecular statics and atomistic kinetic Monte Carlo (AKMC). Molecular statics simulations with a recently developed embedded atom method potential have been carried out in order to obtain atomic configurations, carbon-dislocation binding energies, and the activation energies required for carbon hops in the neighborhood of the line defect. Using information gathered from molecular statics, on-lattice AKMC simulations have been performed for temperatures in the 300–600 K range, so as to study the behavior of a carbon atom as it interacts with the edge dislocation stress field. This model can be seen as a very first step toward the modeling of the kinetics of carbon Cottrell atmosphere formation in iron during the static aging process.

DOI: 10.1103/PhysRevB.82.054103 PACS number(s): 66.30.−h, 05.10.Ln, 61.72.Ff, 07.05.Tp

I. INTRODUCTION

The concept of "atmospheres" (tiny clouds of interstitial impurities that might be found decorating dislocations in crystals) was introduced by Cottrell and Bilby in late 1940s.[1] According to their theory, during the static aging process, carbon atoms in solid solution in an iron matrix diffuse to dislocations because the strain energy is lowered thereby, thus forming what was later called a carbon Cottrell atmosphere. Since they were predicted to pin dislocations, which requires the application of a larger external stress to make them move, Cottrell atmospheres were pointed out as the cause for loss in metal plasticity. Important consequences of dislocation pinning by Cottrell atmospheres, embrittlement, and nonuniform yielding (Lüders bands) may end up being a serious hindrance to manufacture of steel and other metallic alloys. Therefore, formation of Cottrell atmospheres still remains a timely subject in metalurgy.

Cottrell and Bilby roughly estimated the binding energy between an interstitial carbon atom and a dislocation in iron by considering the elastic interaction of the pressure created by the dislocation with the relaxation volume of carbon. Thereafter, more refined analytical models were proposed to overcome the limitations of that pioneering approach, taking into account not only dilatation but also the shear strain associated with impurities,[2] as well as the anisotropy of the cubic cell.[3] Nowadays, with growing computer power, performing large scale numerical simulations that take into consideration the atomistic details of the interaction between both defects became possible as well,[4–10] thus completing the set of tools available for theoretical modeling.

In recent years, three dimension atom probe techniques allowed to obtain images of interstitial impurities distributed around dislocations in metallic alloys,[11–15] providing the missing experimental evidence of Cottrell atmospheres. However, in spite of representing a substantial advance in the experimental side, the actual (i.e., atomic scale) kinetics of impurity diffusion in the neighborhood of a dislocation remains a challenge for these techniques. Macroscopic measurements, e.g., thermoelectric power, on the other hand, have been successfully used to assess the long-time segregation of impurities to dislocations[16,17] but they obviously lack any information at the atomic level. In this context, numerical modeling might come and fill this gap by offering an atomistic view of the kinetics of impurity diffusion near and to dislocations.[8,9]

The aim of the work reported in this article was to model the behavior of a single interstitial impurity in the neighborhood of a dislocation, where the stress field created by the line defect was expected to affect at some extent the impurity diffusion. Given their undisputable technological importance as the main constituents of steel (the most widely used metallic alloy), carbon and iron have been elected the interstitial atom and host material candidates of our model, respectively.

Carbon, in spite of its low solubility in iron, is known to play an important role in the mechanical properties of steel through its interaction with lattice defects, e.g., vacancies, grain boundaries, and, of course, dislocations. Experiments[18] and *ab initio* calculations[19,20] reported that carbon in solid solution should be found occupying an octahedral (o) site in α-iron. On the other hand, the other interstitial position, the tetrahedral (t) site, has been seen to be a transition state according to *ab initio* calculations.[19,20] This draws the general mechanism of carbon migration in a body-centered cubic (bcc) iron matrix as consisting of jumps from an octahedral site to an adjacent octahedral site passing through a tetrahedral site at midway. About dislocations, whose mobility is long believed to give metals the ability of being plastically deformed under stress, there are two basic types, "screw" and "edge,"[21,22] determined by the angle between the line vector and the Burgers vector (either 0° or 90°, respectively; angles in between refer to "mixed" dislocations, which exhibit an intermediary character between the two basic types). In the frame of this work, the edge type has been chosen to be investigated owing to its stress field that possesses both normal and shear components.

In a previous work, Tapasa and co-workers performed a molecular-dynamics (MD) investigation of carbon behavior right in the core of an edge dislocation in α-iron.[6] This paper, in turn, is devoted to the modeling of carbon diffusion in the moderately strained bulklike surroundings of an edge dislocation (the dislocation core itself has not been considered but as a trap for carbon) and thus it covers a much wider area. Molecular dynamics would be, in principle, the most obvious approach to be used for this task as well. Nonetheless, MD has serious known limitations. Concerning time scale, just a few nanoseconds are really feasible with MD since very short-time steps (typically, 10^{-15} s) have to be used during the integration of the equations of motion so as to ensure that the total energy will be conserved. As a consequence of the limited time scale, temperatures much higher than the room temperature are required for MD simulations in solid state, otherwise it is unlikely to observe any diffusion occurring during the simulated time. Last but not least, the number of independent trajectories that can be simulated in a reasonable amount of CPU time with MD is not large enough to allow a meaningful statistical treatment. We rather opted then by coupling two computational approaches, namely, molecular statics and atomistic kinetic Monte Carlo, which allows to simulate thousands of trajectories with duration of up to a few hours at temperatures close to the room temperature (the typical time scale and temperature range of static aging experiments[16,17]), even with a modest hardware. Such a coupling, detailed further, is the basics of the model presented in this work.

II. COMPUTATIONAL APPROACH

A. Atomistic kinetic Monte Carlo

The erratic walk of a carbon atom in a bcc iron matrix is an example of diffusion in solid state. This is one out of many important physical phenomena that are ruled by rare events, i.e., discrete transitions that usually take a long time (compared to atomic vibrations, which are in the order of 10^{13} Hz) to occur. Transition state theory (TST) (Refs. 23–25) states that most of the time the system will be found in the vicinity of a stable state, which is a configuration that corresponds to a local energy minimum in the potential-energy surface. A transition occurs when the system performs a jump to another stable state, adjacent to the current one, surpassing the energy barrier that separates the two states in a sudden move. As such, the long-time evolution of this system can be described in terms of a chain of discrete transitions. Kinetic Monte Carlo (KMC),[26,27] which belongs to the Monte Carlo's family of algorithms that use random numbers to solve a broad range of numerical problems, has been demonstrated to be specially suitable to the study of this kind of state-to-state dynamics. This is in sharp contrast with other Monte Carlo algorithms, such as Metropolis,[28,29] which are time independent and are used to find configurational free-energy minima only.

Among the available KMC algorithms, on-lattice atomistic KMC (AKMC) is one of the simplest.[30] Nonetheless, despite its simplicity, AKMC has been successfully applied to the study of interstitial diffusion in iron[31] and thus it was adopted in this work as well. In typical AKMC, the geometry of the rigid lattice is usually derived from the actual geometry of the system under study. This is to say that, bearing in mind the problem of an interstitial atom (carbon) diffusing in a crystal (bcc iron), every point on the AKMC lattice should correspond to a site in the crystal that is available to be occupied by the interstitial atom. Furthermore, all possible transitions that this kind of system can undergo, as well as their corresponding probabilities, can be found out just once and then tabulated into a reusable event catalog, which enormously speeds up AKMC simulations. Concerning the present model, we have implemented an AKMC code based on the residence time algorithm derived by Young and Elcock for the study of vacancy migration in ordered alloys.[32] A brief description of the algorithm is given below.

The central quantity in AKMC is the residence time, which determines how long the system remains in a given state before jumping to another one. In order to calculate it, all transition probabilities associated with such a state must be known. The probability of occurrence of a transition k during the infinitesimal time interval dt is given by

$$w_k = w_{i\to j} = w_0 P_{i\to j} dt = w_0 \exp\left(\frac{-\Delta E^B_{i\to j}}{k_B T}\right) dt, \qquad (1)$$

where w_0 is the transition attempt frequency (in the order of the atomic vibrations, i.e., 10^{13} Hz), k_B is the Boltzmann constant, T is the simulated temperature, and $\Delta E^B_{i\to j}$ is the energy barrier (at $T=0$ K) to be surpassed in order to the system escapes the current state i to the adjacent state j. According to the TST, the energy barrier for the transition $k \equiv i \to j$ is given by the following simple equation:

$$\Delta E^B_{i\to j} = E^{SP}_{ij} - E_i, \qquad (2)$$

where E^{SP}_{ij} is the total energy of the system at the saddle point (i.e., the transition state) and E_i is the total energy of

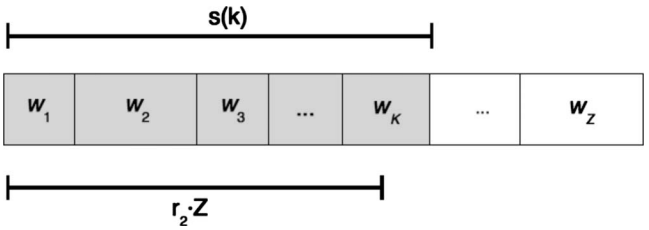

FIG. 1. The Kth transition, whose probability per unit of time is w_K, will be selected since its assigned value of $s(k)$ intercepts $r_2 \cdot Z$.

the system at the state i. Hence, the residence time τ is computed as

$$\tau = -\frac{\ln r_1}{\Omega}, \tag{3}$$

where $\Omega = \Sigma_{k=1}^{Z} w_k$ is the sum of the probabilities of all possible transitions that the system can undergo from the current state and r_1 is a random number between 0 and 1.

As long as τ has been calculated, it is added to the time elapsed until then in order to update the total simulated time, and a transition is selected to make the system advance to the next state. A quantity $s(k) = \Sigma_{k=1}^{K} w_k$ is defined and its value is assigned to the Kth transition, with $K \leq Z$ (Z is the total number of transitions that are allowed from the current state).[33] Then a random number r_2 between 0 and 1 is generated and the transition corresponding to the smallest $s(k)$ that is greater than $r_2 \cdot Z$ will be the chosen one (see Fig. 1).

An important remark is that the energy barriers are entry parameters for AKMC and they can be obtained by a number of methods. Molecular statics was the choice of this work.

B. Molecular statics

Differently from molecular dynamics, which provides the actual evolution of a system of particles in time by integrating Newton's equations of motion, molecular statics comprises a set of methods whose aim is to find out spatial configurations that represent local energy minima in the potential-energy surface. This is to say that molecular statics allows to obtain the ground state of a system (i.e., system configurations for $T=0$ K). As to what concerns the present work, molecular statics simulations have been carried out to obtain relaxed atomic configurations, carbon-dislocation binding energies, and energy barriers for carbon hops in the moderately strained surroundings of an edge dislocation in α-Fe. We used LAMMPS (Ref. 34) with the widely used conjugate gradient method[35] for minimizing the total potential-energy function. Atomic interactions have been described by employing the embedded atom method (EAM) as proposed by Daw and Baskes.[36] In this method, the total energy of an assembly of atoms is obtained by the following equation:

$$E_{tot} = \frac{1}{2}\sum_{i,j} \phi(r_{ij}) + \sum_{i} F_i\left[\sum_{i \neq j} \rho(r_{ij})\right]. \tag{4}$$

Here $\phi(r_{ij})$ is the pairwise interaction between atoms i and j separated by r_{ij}, F_i is the embedding energy of atom i, and $\rho(r_{ij})$ is the electron density induced by atom j at the location of atom i. The Becquart-Raulot EAM potential[37] has been used. The description of the Fe-Fe interactions is based on the well-established Mendelev-Ackland potential[38] whereas the Fe-C part was derived by fitting data from experiments and *ab initio* calculations. This potential reproduces well both the atomic configurations and the minimum-energy path of a carbon atom in perfect α-iron, with the octahedral sites as energy minima and the tetrahedral sites as transition states. The same EAM potential has also been successfully used in simulations where a strained α-Fe crystal was considered.[7,31,37]

C. Saddle-point search

Finding saddle points is not as trivial as finding energy minima, even though there are many different methods available for this purpose.[39] Among these methods, the simplest one is the Drag method, which is very efficient despite being suitable only for the study of simple cases, e.g., single-particle migration in a crystalline lattice. Here we propose a modification of the traditional Drag method that retains the same basic idea of the original one: the system is moved stepwise along a known reaction coordinate, starting from a known energy minimum, being relaxed on the plane perpendicular to the reaction coordinate. The step size is not fixed though. The first step that makes the system leave an energy minimum can be very large (1/3 of the minimum-to-minimum distance, for instance) and the subsequent ones should be smaller (we used 1/10 of that distance as a first guess). At each step, $\vec{F} \cdot d\hat{R}$ is calculated, where $\vec{F}$ is the force vector and $d\hat{R}$ is the unit vector that points from the starting energy minimum to the destination one (i.e., it defines the reaction coordinate). If the scalar product is less than zero, the force is trying to bring the system back to the initial energy minimum and then it has to be dragged in the direction of $d\hat{R}$ in order to climb up the potential-energy surface. On the contrary, if the the scalar product is greater than zero, then the system overpassed the saddle point and is trying to reach the other energy minimum. Then the system is brought back to the previous step, a new step size is defined as half the current one, and the system is moved again toward the second energy minimum. This procedure is iteratively applied until the step size is within an arbitrarily small tolerance or, much less likely, the scalar product $\vec{F} \cdot d\hat{R}$ becomes zero (that is, the system is exactly at the saddle point). It is not possible to draw a minimum-energy path with this method but, on the other hand, this modification is more efficient and accurate to find a saddle point than the traditional Drag method implementation.

III. SIMULATIONS AND RESULTS

A. Energy calculations: Molecular statics

1. Simulation set up

The simulation box for molecular statics comprised around 200,000 iron atoms arranged in a bcc structure [lattice parameter $a_0 = 2.8553$ Å (Ref. 40)] in the following ori-

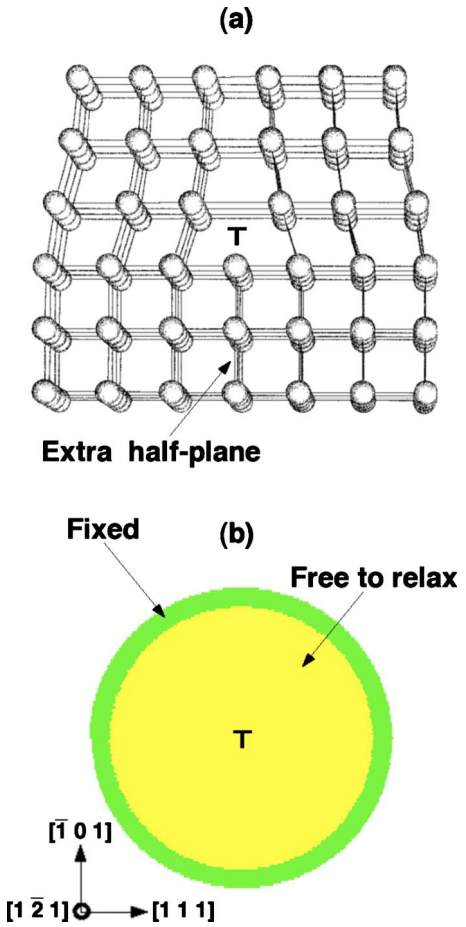

FIG. 2. (Color online) (a) An edge dislocation in a cubic lattice (chosen for the sake of simplicity in the representation). The dislocation line is found in the locus where the extra half-plane ends and is represented by the symbol ⊤. (b) Sketch of the cylindrical simulation box with an edge dislocation right in the center (radius ≈150 Å). The Burgers vector is in the [111] direction and the dislocation line is in the $[1\bar{2}1]$ direction (perpendicular to the plane of the page). The atomic positions in the inner cylinder were allowed to fully relax during molecular statics simulations whereas the positions in the outer ring were kept fixed to the values defined by anisotropic elasticity theory. Periodic boundary conditions were only applied along the dislocation line.

entation: $\vec{u}_x=[111]$, $\vec{u}_y=[\bar{1}01]$, and $\vec{u}_z=[1\bar{2}1]$. The geometry of an edge dislocation is such as if an extra half plane was inserted in the lattice, with the dislocation line being found in the locus where the half-plane ends [Fig. 2(a)]. In order to introduce an edge dislocation in the simulation box, the anisotropic elasticity theory of straight-line defects, initially proposed by Eshelby *et al.*[41] and implemented in the Babel code,[42] has been used to apply to each atom in the iron matrix a displacement corresponding to the Volterra's dislocation elastic field. The dislocation line was oriented parallelly to $\vec{u}_z$ and the Burgers vector was $\vec{b}=a_0/2[111]$. The glide plane was therefore the $(\bar{1}01)$ plane found in the midway between the atomic plane where the extra half plane terminates and the atomic plane just above it. Figure 2(b) presents a sketch of the simulation box, where the first thing to be noticed is that it is cylindrical (radius ≈150 Å) rather than cubic, as usual in computer simulations since the dislocation destroys the periodicity of the lattice. Along the dislocation line (the axis of the cylinder) has been the only direction where periodic boundary conditions have been used. Moreover, the simulation box consisted of an inner cylinder, containing the iron atoms that were allowed to fully relax, surrounded by an outer ring, around 20 Å thick, where the iron atoms were kept frozen in the positions determined by anisotropic elasticity theory. The aim of this rigid boundary condition was to avoid spurious relaxation that might come from free-surface effects, so that the true strain caused by the edge dislocation was permanently reproduced in the boundary of the simulation box.

Within this simulation box, one can discern two distinct regions. The largest one looks like the perfect bulk bcc iron and carbon diffusion in this region is expected to operate according to the same mechanism (jumps from/to neighboring o sites). The other region is the dislocation core itself, where lattice distortion is so high that the bcc symmetry is not observed anymore. In order to define the dislocation core region, the centrosymmetry deviation (CSD) parameter[43] was employed.

The CSD parameter is a simple way to measure how a centrosymmetric crystal, such as bcc iron, is locally distorted by a defect. In a centrosymmetric crystal, for every atomic position, there is a first nearest neighbor at $\vec{r}_i$ and another one at $\vec{r}_j=-\vec{r}_i$, so that $(\vec{r}_i+\vec{r}_j)^2=0$. The CSD parameter of an atom in the matrix is then obtained by summing over all the pairs of opposite nearest neighbors of such an atom, and it is straighforward to see that CSD=0 everywhere in a crystal that is either perfect or under homogeneous deformation (dilation or contraction). If a defect is present, on the other hand, the material suffers a nonelastic deformation and the equal and opposite relation described above is no longer valid for all of the nearest-neighbor pairs of the atoms that are close to the defect. By calculating the CSD parameter, one can localize the atoms that form the dislocation core. The CSD mapping in the vicinity of an edge dislocation in α-iron is shown in Fig. 3. As expected, the CSD becomes larger as the iron atoms are closer to the dislocation line. Not very far away though, the CSD parameter rapidly goes close to zero, which means that typical bcc symmetry is kept almost unchanged. The iron atoms in the dislocation core region have been defined as the ones with a CSD parameter larger than 0.5 $Å^2$.

Both the stable state and the transition state for carbon in α-Fe correspond to interstitial sites in the host crystal, respectively, the octahedral site and the tetrahedral site. Since the main purpose of molecular statics in the context of our model is to obtain energy barriers for carbon jumps (Eq. (5)), it was necessary first to map all the interstitial sites in the area of interest, that is, the surroundings of the line defect, out of the dislocation core (where such a mapping is meaningless), in order to check if they remain energy minima and saddle points in a moderately strained lattice. In strain-free bcc iron, an octahedral site is found in the midpoint of every pair of neighboring iron atoms oriented along one of the tetragonal distortion axes ([100], [010], or [001]). A tetrahedral site, in turn, is always found in the midpoint of two

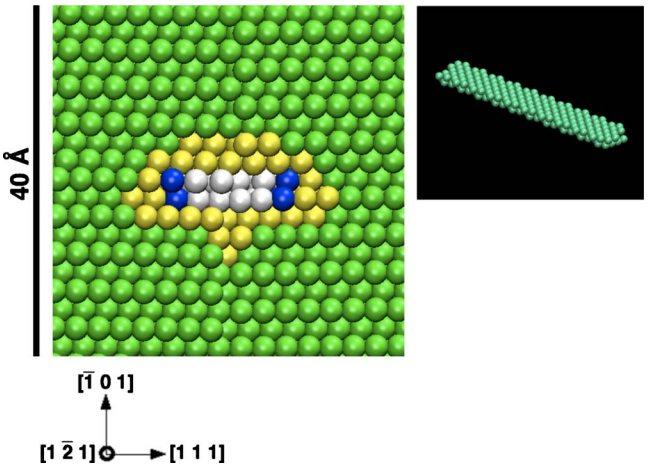

FIG. 3. (Color online) Centro-symmetry deviation mapping in the vicinity of an edge dislocation in α-Fe: [green (mid gray) balls] CSD<0.005 Å^2, [yellow (light gray) balls] $0.005 \leq$CSD <0.05 Å^2, [blue (dark gray) balls] $0.05 \leq$CSD<0.5 Å^2, and (white balls) CSD≥ 0.5 Å^2. In the inset, the iron atoms in the dislocation core (side view), i.e., atoms with a CSD parameter larger than 0.5 Å^2.

adjacent octahedral sites. Following the convention adopted by Garruchet and Perez,[31] the o sites were, respectively, labeled type 1, type 2, or type 3 depending on the Fe-Fe pair orientation. In the above defined simulation box, all o sites within a region of radius 100 Å around the dislocation line were mapped. Therefore, there was at least a distance of 30 Å (around six times the interatomic potential cutoff) separating a mapped interstitial position and the rigid layer depicted in Fig. 2(b). It was then straightforward to map also the t sites. The t sites were labeled in the same way as the o sites, so that a t site of type 1 sits on the midpoint between a type 2 and a type 3 o site (which, as a pair, are oriented along the [100] direction), and so on. Interstitial positions right in the dislocation core region have not been considered in this work.

2. Dislocation stress field

Before introducing an interstitial carbon atom, the simulation box has been relaxed by molecular statics. The relaxed dislocation core was straight (that is, it did not exhibit any kink), staying in the center of the simulation box. After relaxation, except in the vicinity of the dislocation core, the atomic coordinates did not differ more than a few hundredths of angstrom from the initial coordinates provided by anisotropic elasticity theory, confirming once again the ability of this theory to predict atomic positions wherever lattice strain is moderate. The resulting strain is the source of a long-range internal stress field, the mapping of the nonzero components of which is depicted in Fig. 4. As one can see, both normal and shear stress components are present. Acting parallelly to the Burgers vector, σ_{xx} is the largest component of normal stress and splits the simulation box into two regions: one above the glide plane where the stress is positive (tensile) and other below it where stress is negative (compressive). The only relevant component of shear stress is σ_{xy} but it is remarkable only in the region close to the glide plane. As there is no important contribution to the stress field along the z axis (parallel to the dislocation line), σ_{zz}, σ_{xz}, and σ_{yz} vanishes very quickly out of the dislocation core.

3. Energy minima and saddle-point energies

The simple mechanism accepted so far for carbon diffusion in perfect bcc iron yields three possible directions for carbon jumps: $1 \rightleftarrows 2$ (along the [001] direction), $1 \rightleftarrows 3$ (along the [010] direction), and $2 \rightleftarrows 3$ (along [100] direction), where 1, 2, and 3 are o-site types. These directions, taking into consideration the simulation box orientation, are given by the following unit vectors: $\hat{u}_{[100]}=(\sqrt{3}/3,-\sqrt{2}/2,\sqrt{6}/6)$, $\hat{u}_{[010]}=(\sqrt{3}/3,0,-\sqrt{6}/3)$, and $\hat{u}_{[001]}=(\sqrt{3}/3,\sqrt{2}/2,\sqrt{6}/6)$. We have employed the modified Drag method presented in Sec. II to search for energy minima and saddle points on the lines shown in Fig. 5(a), which are oriented along the [100], [010], and [001] directions and crossed each other right in the dislocation core.

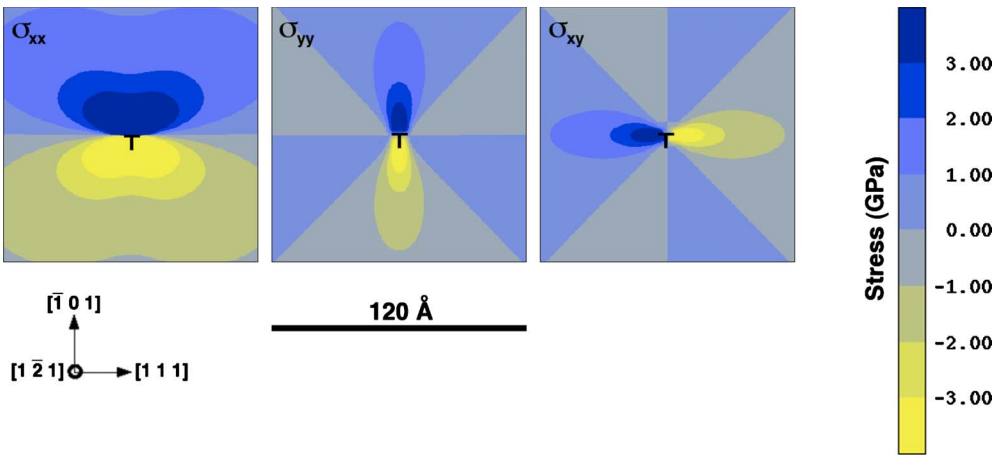

FIG. 4. (Color online) The three nonzero (out of the dislocation core) components of the edge dislocation stress field (plot area: 120×120 Å^2), as calculated by molecular statics.

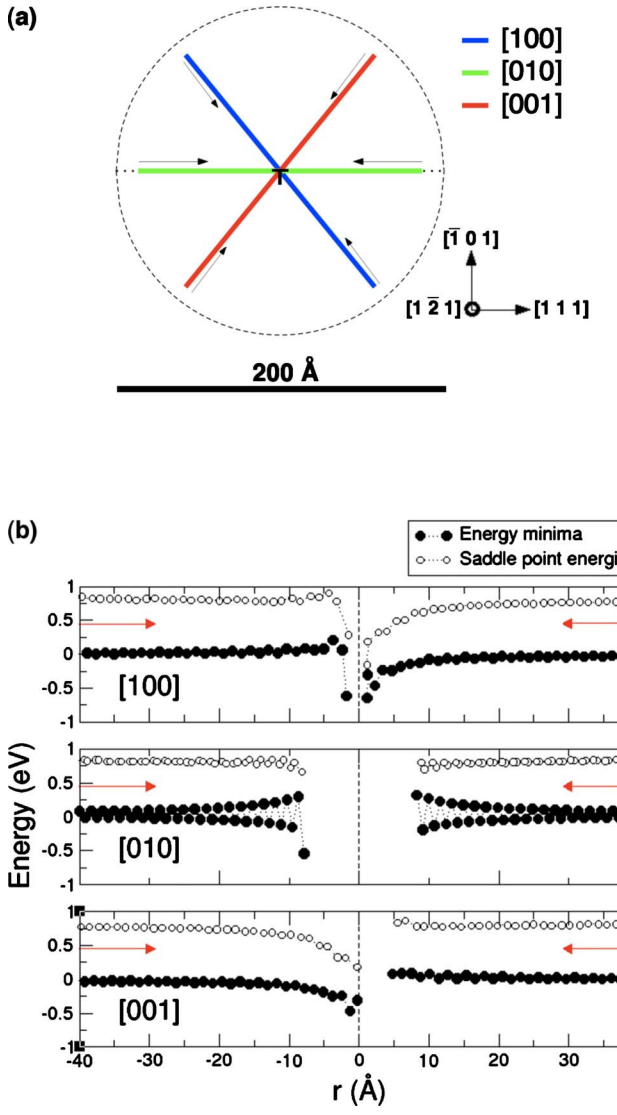

FIG. 5. (Color online) (a) [100], [010], and [001] directions (taken with respect to the dislocation line) where saddle-point search with the modified Drag method has been carried out. The dotted line indicates the glide plane, and the dashed circle (whose radius is 100 Å) encompasses the region where octahedral and tetrahedral sites have been mapped. (b) Local energy minima (filled circles) and saddle points (empty circles) along the [100], [010], and [001] directions, as obtained with the modified Drag method. The energy reference is the total energy of the o site in the corresponding line end. The dashed line indicates the position of the dislocation line.

After defining the search lines as stated in the precedent paragraph, the simulations with the modified Drag method have been carried out in the following way. First, all octahedral and tetrahedral sites lying on the lines shown in Fig. 5(a) have been found. Then, for each line, a carbon atom was initially placed in the o site located in one of the line ends (around 80 Å away from the dislocation line), full energy minimization was performed and the atom was dragged toward the first saddle point on the line. During saddle-point search, only the carbon atom has been constrained, with all of its degrees of freedom being supressed except on the plane

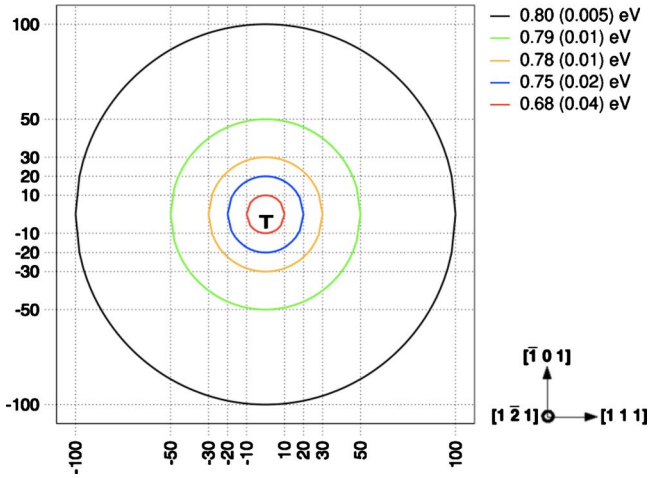

FIG. 6. (Color online) Mean energy barriers inside the molecular statics simulation box. The dispersion (standard deviation) about the mean is in parentheses. The activation energy at $T=0$ K in a nonstrained bcc iron lattice obtained with the with the current EAM potential is 0.81 eV.

perpendicular to the corresponding search direction. As long as a saddle point was found, the carbon atom was moved a small distance along the line and allowed to fully relax in order to go down to the next energy minimum. This procedure has been repeated up to the carbon arrived to the dislocation core, and then restarted at the opposite line end (see where the arrows point to in the same picture). Figure 5(b) presents the energy minima (filled circles) and saddle-point energies (empty circles) along the three search directions (the energy reference is the total energy of the o site in the corresponding line end). The gaps in the plots in Fig. 5(b) were due to the modified Drag method not being able to find out a saddle point by following the respective search direction, which, not surprisingly, only occurs when the carbon atom gets close to the dislocation core.

In these simulations, most of times the energy minima and saddle points have matched the o- and t-site positions distributed on the search lines, respectively, with minor deviations near the dislocation core. Based on theses results, we have assumed that, outside the dislocation core, in the bulklike region, the o sites remained the stable states for carbon and the t sites, the saddle points. Regarding the molecular statics simulations, when initially placed in an o-site, the carbon atom was allowed to fully relax, while in a t site, it was allowed to relax only on the plane perpendicular to the line connecting the two associated o sites. Energy minimization has been carried out in both cases up to the relative change in the energy was less than 10^{-10}, a criterion fine enough to achieve a well converged geometry. It is worthwhile to say that this mapping of energy minima and saddle-point energies required more than 160,000 molecular statics simulations, one for each mapped interstitial site. Then, by applying Eq. (2), all the energy barriers for carbon hops inside the simulation box have been calculated. The mean energy barriers for different distances from the dislocation line are depicted in Fig. 6. As an overall effect, one can see that the closer to the edge dislocation, the lower the mean energy barriers for carbon diffusion.

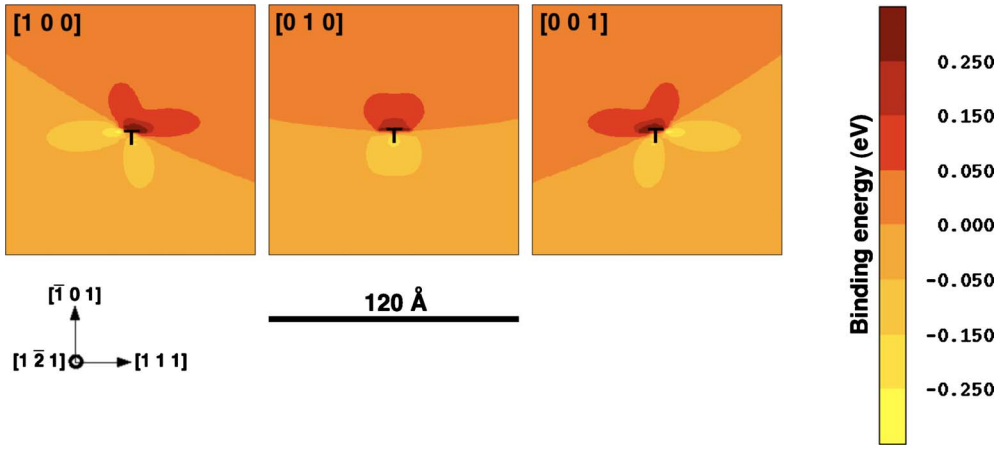

FIG. 7. (Color online) Mapping of carbon-dislocation binding energies per octahedral site type in the neighborhood of an edge dislocation (plot area: 120×120 Å^2).

Besides the calculation of energy barriers for AKMC, the energy minima and saddle-point energies obtained with molecular statics simulations also allowed to characterize (1) the strength and range of carbon-dislocation interactions, and (2) how carbon diffusion is biased due to the presence of the line defect. These results are summarized below.

4. Carbon-dislocation interactions

Binding energies provide a measure of the type (whether energetically favorable or not) and strength of the interaction between two entities in a system at $T=0$ K (i.e., a local energy minimum in the potential-energy surface). The binding energy between a carbon atom and the edge dislocation was calculated as follows:

$$\Delta E^b = [E_{dislo} + E_C] - [E_{dislo,C} + E_{ref}]. \quad (5)$$

In this equation, E_{dislo} is the total energy of the simulation box with an edge dislocation and no carbon atom, E_C is the total energy of the simulation box with a carbon atom in an o site (stable position) without dislocation, $E_{dislo,C}$ is the total energy of the simulation box with both defects and E_{ref} is the simulation box without any defect.

Figure 7 shows the mapping of the carbon-dislocation binding energies as a function of carbon position with respect to the dislocation line. Not surprisingly, the most attractive (positive) binding energies are found just above the dislocation core, in the tensile half whereas just below the dislocation core the carbon-dislocation interaction has a repulsive character (negative binding energies). One can see that the binding energies depend not only on the carbon-dislocation distance but also (and mainly) on the angle with respect to the glide plane, confirming what pioneering models predicted a long-time ago.[1,2] Moreover, looking at the mapping of the edge dislocation stress field in Fig. 4, the relationship between the nonzero stress components and the binding energies is clarified. For instance, one can see that the interaction of a carbon atom in a type 2 o site with the edge dislocation along the glide plane is almost negligible ($\Delta E^b \approx 0$ eV) even a few angstrom only away from the line defect since this interstitial position is quite insensitive to the shear stress that predominates there. However, it would suffice carbon jumps to a neighboring type 1 or type 3 o site to be in either a favorable or unfavorable position since these site types are differently affected by shear.

Considering that thermal energy is available ($T>0$ K), one can estimate how far from the dislocation line a carbon atom still is importantly affected by the presence of the line defect by verifying whether $|\Delta E^b| > k_B T$, where $|\Delta E^b|$ is the absolute value of the carbon-dislocation binding energy (see Fig. 8). For $T=300$ K, the region where carbon-dislocation elastic interaction still beats thermal energy has the shape of a four-leaf clover and has a maximum width of 145 Å and a maximum height of 100 Å. Of course, this region is reduced as the temperatuture increases, so, taking into account the temperature range investigated in this work (300–600 K), we can safely assume that the size of the simulation box we have used is large enough to handle the relevant interactions between both defects.

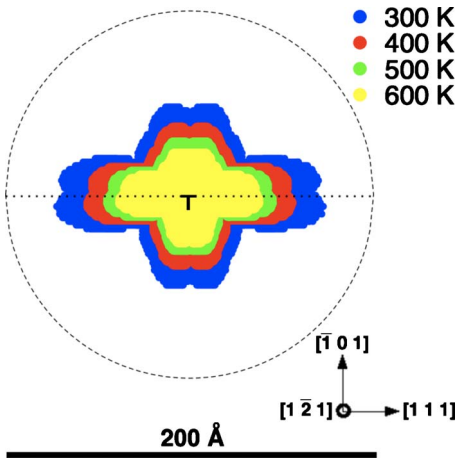

FIG. 8. (Color online) Region containing sites for which $|\Delta E^b| > k_B T$, for different temperatures. The dotted line indicates the glide plane, and the dashed circle (whose radius is 100 Å) indicates the boundary of the region of the simulation box where octahedral and tetrahedral sites have been mapped.

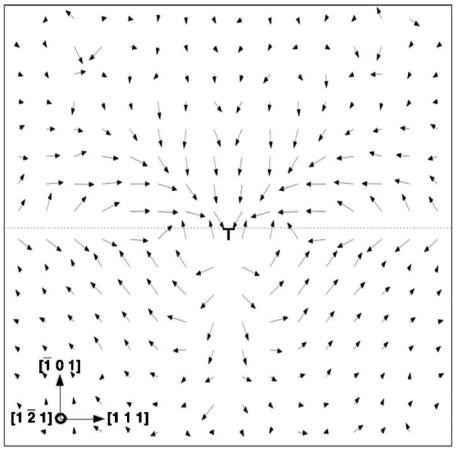

FIG. 9. Average vectors $\langle\vec{\epsilon}\rangle$ in a 20×20 mesh ($\Delta x=\Delta y=10$ Å), for $T=300$ K. Only the components perpendicular to the dislocation line are shown, in order to characterize how carbon diffusion is biased with respect to the line defect. Arrows have been rescaled to make visualization easier (10 Å$\equiv a0/2$). The longest the arrow, the strongest the bias on carbon diffusion.

5. Dislocation-induced bias on carbon diffusion

When it diffuses in a perfect bcc iron matrix, a carbon atom can be seen as a simple random walker: once occupying an o site, the probability that it jumps to one of the four neighboring o sites (25%) and the step length ($a_0/2$) are the same for all possible transitions. On the other hand, if the lattice is nonhomogeneously strained, as is the case when an edge dislocation is present, the energy of the different o and t sites change and, as a consequence, the relative heights of the energy barriers (and thus, transition probabilities) change as well. Carbon diffusion is now better described as a biased random walk (BRW).[44–46] In contrast with a simple random walk (SRW), one can observe a net drift on average in specific directions in a BRW. A vector $\vec{\epsilon}$ (mean displacement vector), the aim of which is to provide a measure of this drift, can be defined as

$$\vec{\epsilon}=\sum_{j=1}^{N} P_{i\to j}\vec{\delta}_{i\to j}=\sum_{j=1}^{N}\exp\left(-\frac{\Delta E^{B}_{i\to j}}{k_B T}\right)\vec{\delta}_{i\to j}, \qquad (6)$$

where $\Delta E^{B}_{i\to j}$ is the energy barrier for the transition $i\to j$, $\vec{\delta}_{i\to j}$ is the vector that connects the o site i to j and $N=4$ is the number of first nearest neighbors of site i. It is straightforward to see that the length of $\vec{\epsilon}$ varies from 0 (no net displacement, as is the case for a perfect random walk) up to around $a_0/2$ (as when the probability of one of the four possible transitions approaches 100% and the walk is not random anymore).

Figure 9 presents the average vectors $\langle\vec{\epsilon}\rangle$ in a 20×20 mesh (therefore, $\Delta x=\Delta y=10$ Å), for $T=300$ K, and offers an intuitive picture of the effect of the stress field of the edge dislocation on carbon diffusion. Only the components perpendicular to the dislocation line are shown. As can be seen, an edge dislocation induces a quite complex bias on carbon diffusion, depending not only on the proximity with the dislocation core but also on the region (compression or tensile). Above the glide plane, the "wind" clearly leads carbon, with more or less intensity, directly to the core region. The picture changes below the glide plane, where the carbon tends to avoid the dislocation core and is more likely to rather move toward the glide plane. In the vicinity of the glide plane, where σ_{xy} (shear) is the predominant component of the dislocation stress field, the carbon atom falls into a channel that on average takes it to the dislocation core.

B. Carbon diffusion in the vicinity of the edge dislocation: AKMC simulations

1. Simulation set up

The AKMC simulation box was derived from the simulation box used for molecular statics in such a way that every point on the rigid lattice of the first corresponded to one of the mapped octahedral sites in the latter. The AKMC lattice can thus be seen as a network of octahedral sites interconnected by transition states (tetrahedral sites). Starting positions have been randomly chosen in all AKMC simulations. Moves on the lattice have been constrained so that carbon hops have been allowed only between nearest-neighbor sites. Energy barriers have been calculated by Eq. (2) with the energy minima and saddle-point energies obtained by molecular statics simulations. Two end points have been defined for the AKMC simulations. The first one was the dislocation core, taken as a single (and special) point on the rigid lattice, an "absorbing" site. Once there, the carbon atom is considered trapped and taken out of the simulation.[47] The second end point was the boundary of the AKMC simulation box, a cylinder such as the molecular statics one. The lack of periodic boundary conditions in the directions perpendicular to the dislocation line implied that a carbon atom could be lost during the course of an AKMC simulation just by leaving the AKMC simulation box through the open boundary. In such a case, given the maximum range of effective carbon-dislocation interaction for the lowest considered temperature (see Fig. 8), we may actually conclude that these lost carbon atoms have completely escaped the influence of the dislocation stress field. In other words, close to the boundary of the simulation box, the edge dislocation did not play any noticeable role on carbon diffusion anymore.

Temperatures in the 300–600 K range have been simulated by AKMC, yielding a total of 500 000 simulations per temperature. Every individual AKMC simulation yielded an independent carbon trajectory in the neighborhood of the edge dislocation. Carbon concentration was assumed to be very low, so that carbon-carbon interactions, since very unlikely, could be safely neglected. For the purpose of highlighting the effect of the dislocation-induced bias on carbon diffusion, some of the results of biased random walk AKMC have been compared to the ones of simple random walks. AKMC simulations of SRWs have been performed by considering that all transitions had the same energy barrier of 0.81 eV everywhere.

2. Carbon diffusivity

Initially, the diffusion coefficient of the carbon atom in a perfect bcc iron lattice has been calculated by applying the

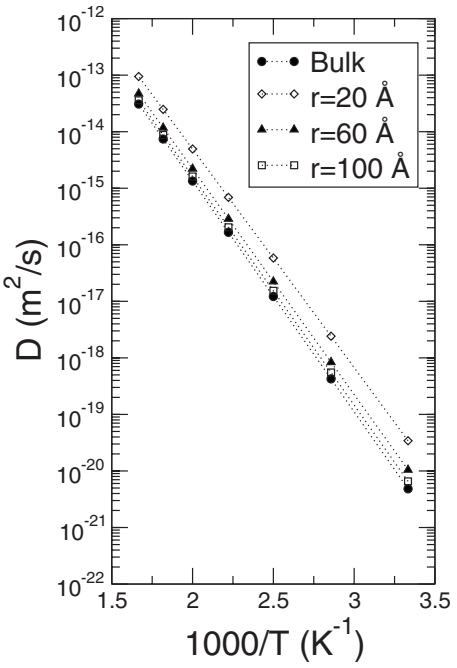

FIG. 10. Mean diffusion coefficient as a function of volume (delimited by the radius r, see Eq. (7)) compared to bulk diffusivity. Considering the whole volume of the AKMC simulation box, the mean diffusion coefficient tends do the bulk value for all temperatures.

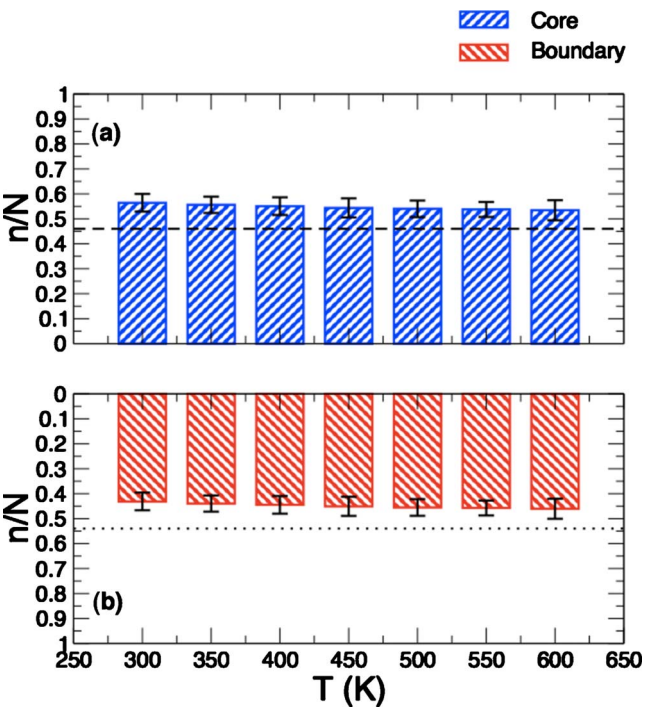

FIG. 11. (Color online) Fraction of total carbon trajectories that (a) terminated in the core of the edge dislocation or (b) left the AKMC simulation box through its open boundaries. The dashed (dotted) line indicates the fraction of trajectories that should arrive to the dislocation core (simulation box boundary) if bias on carbon diffusion is not considered.

well-known Einstein's formula $\langle r^2\rangle = 6Dt$, where $\langle r^2\rangle$ is the mean squared displacement, so that we could compare to the diffusion coefficient in the surroundings of the edge dislocation. However, since the energy barriers change depending on carbon location in the strained iron lattice, the diffusion coefficient is not constant anymore. The mean (effective) carbon diffusivity inside a number of cylindrical volumes—whose axis corresponded to the edge dislocation line—of different radii has been calculated as follows:

$$\bar{D}(r) = \frac{\bar{\delta}^2}{6\bar{\tau}}, \tag{7}$$

where $\bar{\tau}$ and $\bar{\delta}$ are, respectively, the mean residence time and the mean jump distance inside the volume delimited by r. Only carbon trajectories restricted to the specified volumes were included in the corresponding averages. The dislocation core, in turn, was not included.

Arrhenius plots of $\bar{D}$ for different cylinder radii are shown in Fig. 10. Inside the cylinder of $r=20$ Å, at $T=300$ K, $\bar{D}$ is around one order of magnitude higher than D_{bulk} (namely, the diffusion coefficient of carbon in a nonstrained α-Fe lattice). However, as $\bar{D}$ seems to vary proportionally to $1/r^2$, $\bar{D} \to D_{bulk}$ very quickly. Considering the whole AKMC simulation box ($r=100$ Å), one can see that $\bar{D} \approx D_{bulk}$ for all the considered temperatures, thus indicating that the contribution of the edge dislocation stress field (out of the core) to the effective diffusivity is negligible.[48] Dislocation contribution to the effective carbon diffusivity should rather come from the diffusivity right in the dislocation core, which can be many orders of magnitude higher than bulk diffusivity.[49]

3. Analysis of carbon trajectories

If bias on carbon diffusion is not taken into account, the edge dislocation has a neutral character with relation to the interstitial atom. In this case, trapping occurs purely by chance when the carbon atom falls into the dislocation core in the course of a SRW. Since Fig. 6 revealed that carbon diffusion is effectively biased owing to the presence of the line defect, it is worth knowing if such a bias contributes or not to favor carbon trapping compared to the SRW case (this is not clear just by inspection). Figure 11 depicts the fraction of carbon trajectories that either terminated in the dislocation core or left the simulation box through its open boundary. The dashed and dotted lines represent the mean values given by SRW simulations. As one can see, the amount of trajectories that arrived to the dislocation core in BRW simulations not only increased compared to the unbiased case but they became the majority (53–56 % against 46%). Otherwise stated, the edge dislocation presented a slightly attractive character.

As also featured in Fig. 9, sharp contrasts are drawn between bias on carbon diffusion below and above the glide plane (in the vicinity of which the shear stress σ_{xy} is significative). In the AKMC simulations, the glide plane has been thus defined as an interface separating the two diffusion regimes of carbon. We verified that it is relatively common a

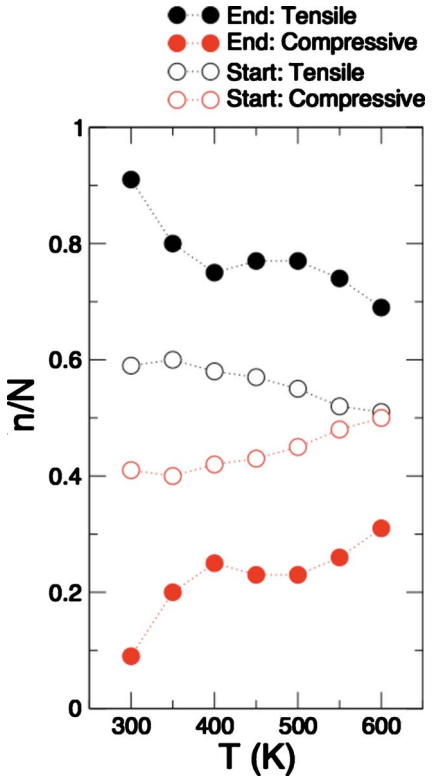

FIG. 12. (Color online) (Empty circles) Fraction of dislocation-trapped carbon trajectories starting in either the tensile or the compressive half. (Filled circles) Fraction of dislocation-trapped carbon trajectories that arrived to the dislocation core coming from either the tensile or the compressive half.

carbon trajectory starting in one half to cross the glide plane toward the other one. Indeed, at $T=300$ K, a trajectory has crossed the glide plane about 20 times on average (15, in the SRW simulations). However, instead of going deeply inside the other half of the simulation box, as has been common in the SRWs, the carbon atom rather preferred to stay in the vicinity of the glide plane: in around 44% of the time elapsed after arriving there, the interstitial atom has been found inside a stripe delimited by the third planes above and below the glide plane.

An interesting point is raised by Fig. 12. At $T=300$ K, for instance, 90% of the dislocation-trapped trajectories approached the dislocation core coming from the tensile half, even though 40% of these trajectories started in the compressive one. Therefore, a carbon atom diffusing in the compressive half is much more likely to cross the glide plane toward the tensile half rather than to go directly to the dislocation core. Moreover, the vicinity of the glide plane actually works as a channel through which a carbon atom is driven toward the dislocation core. The amount of carbon trajectories that arrived to the dislocation core after falling into the shear stress field was in the 79–82 % range in the BRWs (about 10% more than what was found in the SRWs). On the other hand, 2/3 of the trajectories that started in the tensile half and terminated in the dislocation core have not crossed the glide plane any time, thus indicating that carbon diffused directly toward the dislocation core.

From the analysis of the biased random walks, it was also possible to estimate a capture radius, i.e., a distance from the dislocation line that delimited a semicircle in the tensile half inside which almost 100% of the entering carbon trajectories terminated in the dislocation core. The capture radius is obviously temperature dependent. For $T=300$ K, the lowest temperature of this study, we have found a capture radius of around 40 Å. In turn, for the highest considered temperature, 600 K, the capture radius was of only 15 Å.

4. Blocking the dislocation core

In the AKMC simulations presented just above, there were no obstacles in the path of the carbon atom, so that once captured by the dislocation stress field, it diffused to the dislocation core and was trapped there. A question that may be posed is: what if the dislocation core was saturated and thus it could not absorb any new arriving carbon atom? A hundred of extra AKMC simulations have been carried out in order to specifically clarify this point. The starting point of all carbon trajectories has been defined to be the same, located at around 30 Å right above the dislocation core. In these simulations, performed at $T=300$ K, the core has been blocked to the carbon atom. Prevented from entering the dislocation core, the carbon atom exhibited a "fly-around-a-lamp" behavior: in all simulations, the carbon atom first moved toward the dislocation core, as expected, and then started to jump around it. In quantitative terms, in more than 70% of the total simulated time, the carbon atom was found diffusing within a distance of 10 Å from the dislocation line. (The probability reaches 95% if the considered distance is 20 Å.) Even after 100 000 steps, no carbon trajectory moved away and left the simulation box through the open boundary.

IV. CONCLUSIONS

In summary, this paper presented a simple model to investigate the behavior of a single interstitial impurity (carbon) diffusing in the matrix of a bcc metal (iron) strained owing to the presence of a line defect (edge dislocation). We employed molecular statics with an EAM potential to obtain energy barriers in order to feed an atomistic kinetic Monte Carlo code, used to generate a number of independent trajectories of the interstitial atom. Temperatures in the 300–600 K range were considered. Carbon diffusion near an edge dislocation is a sort of biased random walk, with location dependent transition probabilities. In the compressive half, the carbon atom is repelled by the dislocation core and either it moves in oblique trajectories toward the glide plane (where it may be driven by the shear stress to the dislocation core) or even escapes the influence of the edge dislocation, moving away from the trap. On the other hand, in the tensile half, the carbon atom is more likely to diffuse directly toward the dislocation core. Two diffusion regimes for carbon in the neighborhood of the edge dislocation can be discerned thereby.

ACKNOWLEDGMENTS

R.G.A.V. acknowledges Electricité de France (EDF) for funding. This work used computational facilities provided by the P2CHPD cluster at Université Claude Bernard, Lyon, France. Partial support of "Agence Nationale de la Recherche" on CONTRAPRECI project (06-BLAN-0205) is gratefully acknowledged.

[1] A. H. Cottrell and B. A. Bilby, Proc. Phys. Soc. A **62**, 49 (1949).
[2] A. W. Cochardt, G. Shoek, and H. Wiedersich, Acta Metall. **3**, 533 (1955).
[3] R. M. Douthwaite and J. T. Evans, Scr. Metall. **7**, 1019 (1973).
[4] E. Clouet, Acta Mater. **54**, 3543 (2006).
[5] Y. Niu, S.-Y. Yang, D.-L. Zhao, and C.-Y. Wang, J. Phys.: Condens. Matter **13**, 4267 (2001).
[6] K. Tapasa, Y. N. Osetsky, and D. J. Bacon, Acta Mater. **55**, 93 (2007).
[7] E. Clouet, S. Garruchet, H. Nguyen, M. Perez, and C. S. Becquart, Acta Mater. **56**, 3450 (2008).
[8] C. Hin, Y. Bréchet, P. Maugis, and F. Soisson, Acta Mater. **56**, 5535 (2008).
[9] A. Ramasubramaniam, M. Itakura, M. Ortiz, and E. A. Carter, J. Mater. Res. **23**, 2757 (2008).
[10] S. Taketomi, R. Matsumoto, and N. Miyazaki, J. Mater. Sci. **43**, 1166 (2008).
[11] L. Chang, Ph.D. thesis, Oxford University, 1985.
[12] D. Blavette, E. Cadel, A. Fraczkiewicz, and A. Menand, Science **286**, 2317 (1999).
[13] E. Cadel, D. Lemarchand, A.-S. Gay, A. Fraczkiewicz, and D. Blavette, Scr. Mater. **41**, 421 (1999).
[14] J. Wilde, A. Cerezo, and G. D. W. Smith, Scr. Mater. **43**, 39 (2000).
[15] K. Thompson, P. L. Flaitz, P. Ronsheim, D. J. Larson, and T. F. Kelly, Science **317**, 1370 (2007).
[16] N. Lavaire, J. Merlin, and V. Sardoy, Scr. Mater. **44**, 553 (2001).
[17] N. Lavaire, V. Massardier, and J. Merlin, Scr. Mater. **50**, 131 (2004).
[18] D. A. Porter and K. E. Easterling, *Phase Transformations in Metals and Alloys*, 2nd ed. (Chapman and Hall, London, 1981).
[19] D. E. Jiang and E. A. Carter, Phys. Rev. B **67**, 214103 (2003).
[20] C. Domain, C. S. Becquart, and J. Foct, Phys. Rev. B **69**, 144112 (2004).
[21] V. Bulatov and W. Cai, *Computer Simulations of Dislocations* (Oxford University Press, New York, 2006).
[22] J. P. Hirth and J. Lothe, *Theory of dislocations* (McGraw-Hill, New York, 1968).
[23] R. Marcelin, Ann. Phys. **3**, 120 (1915).
[24] E. Wigner, Z. Phys. Chem. **19**, 203 (1932).
[25] H. Eyring, J. Chem. Phys. **3**, 107 (1935).
[26] A. F. Voter, F. Montalenti, and T. C. Germann, Annu. Rev. Mater. Res. **32**, 321 (2002).
[27] K. A. Fichthorn and W. H. Weinberg, J. Chem. Phys. **95**, 1090 (1991).
[28] N. Metropolis, A. W. Rosenbluth, M. N. Rosenbluth, A. H. Teller, and E. Teller, J. Chem. Phys. **21**, 1087 (1953).
[29] D. Frenkel and B. Smit, *Understanding Molecular Simulation—From Algorithms to Applications* (Academic Press, New York, 2002).
[30] C. S. Becquart and C. Domain, Phys. Status Solidi B **247**, 9 (2009).
[31] S. Garruchet and M. Perez, Comput. Mater. Sci. **43**, 286 (2008).
[32] W. M. Young and E. W. Elcock, Proc. Phys. Soc. **89**, 735 (1966).
[33] A. B. Bortz, M. H. Kalos, and J. L. Lebowitz, J. Comput. Phys. **17**, 10 (1975).
[34] S. J. Plimpton, J. Comput. Phys. **117**, 1 (1995).
[35] J. R. Shewchuk, An introduction to the conjugate gradient method without the agonizing pain, 1994.
[36] M. S. Daw and M. I. Baskes, Phys. Rev. Lett. **50**, 1285 (1983).
[37] C. S. Becquart, J. M. Raulot, G. Benecteux, C. Domain, M. Perez, S. Garruchet, and H. Nguyen, Comput. Mater. Sci. **40**, 119 (2007).
[38] G. J. Ackland, M. I. Mendelev, D. J. Srolovitz, S. Han, and A. V. Barashev, J. Phys.: Condens. Matter **16**, S2629 (2004).
[39] G. Henkelman, G. Jóhannesson, and H. Jónsson, *Progress on Theoretical Chemistry and Physics* (Kluwer Academic, Alphen aan den Rijn, the Netherlands, 2000), Chap. 10.
[40] This is the equilibrium lattice parameter of bcc iron obtained with the Becquart-Raulot interatomic potential at 0 K.
[41] J. D. Eshelby, W. T. Read, and W. Shockley, Acta Metall. **1**, 251 (1953).
[42] Provided by E. Clouet, CEA-Saclay, France.
[43] C. L. Kelchner, S. J. Plimpton, and J. C. Hamilton, Phys. Rev. B **58**, 11085 (1998).
[44] J. Rudnick and G. Gaspari, *Elements of the Random Walk* (Cambridge University Press, Cambridge, 2004), Chap. 5.
[45] V. R. Barlett, J. J. Bigeón, M. Hoyuelos, and H. O. Mártin, J. Comput. Phys. **228**, 5740 (2009).
[46] E. A. Codling, M. J. Plank, and S. Benhamou, J. R. Soc., Interface **5**, 813 (2008).
[47] Indeed, the interstitial atom is expected to diffuse in the narrow channel of the dislocation core now but this "pipe diffusion" has not been investigated in this work.
[48] In fact, the dislocation-to-dislocation distance, for typical dislocation densities, can be on the order of 10^3 Å, by far larger than the AKMC simulation box radius used in this work.
[49] H. Mehrer, *Diffusion in Solids: Fundamentals, Methods, Materials, Diffusion-Controlled Processes* (Springer, New York, 2007), Chap. 33.